

Engineering metal oxide nanostructures for the fiber optic sensor platform

Zsolt L. Poole,¹ Paul Ohodnicki,² Rongzhang Chen,¹ Yuankun Lin,³
and Kevin P. Chen^{1,*}

¹Department of Electrical and Computer Engineering, University of Pittsburgh Pittsburgh, PA, 15261, USA

²National Energy Technology Laboratory, 626 Cochran Mill Road, Pittsburgh, PA 15236, USA

³Department of Physics, University of North Texas, Denton, TX 76203, USA

*pec9@pitt.edu

Abstract: This paper presents an effective integration scheme of nanostructured SnO₂ with the fiber optic platform for chemical sensing applications based on evanescent optical interactions. By using a triblock copolymer as a structure directing agent as the means of nano-structuring, the refractive index of SnO₂ is reduced from >2.0 to 1.46, in accordance with effective medium theory for optimal on-fiber integration. High-temperature stable fiber Bragg gratings inscribed in D-shaped fibers were used to perform real-time characterization of optical absorption and refractive index modulation of metal oxides in response to NH₃ from the room temperature to 500°C. Measurement results reveals that the redox reaction of the nanostructured metal oxides exposed to a reactive gas NH₃ induces much stronger changes in optical absorption as opposed to changes in the refractive index. Results presented in this paper provide important guidance for fiber optic chemical sensing designs based on metal oxide nanomaterials.

©2014 Optical Society of America

OCIS codes: (060.0060) Fiber optics and optical communications; (160.4236) Nanomaterials; (280.0280) Remote sensing and sensors.

References and links

1. S. Akbar, P. Dutta, and C. Lee, "High-temperature ceramic gas sensors: a review," *Int. J. Appl. Ceram. Tec.* **3**(4), 302–311 (2006).
2. G. Korotcenkov, "Gas response control through structural and chemical modification of metal oxide films: state of the art and approaches," *Sens. Actuators B Chem.* **107**, 209–232 (2005).
3. G. Korotcenkov, "Metal oxides for solid-state gas sensors: What determines our choice?" *Mat. Sci. Eng. B Solid.* **139**(1), 1–23 (2007).
4. N. Yamazoe, "Toward innovations of gas sensor technology," *Sens. Actuators B Chem.* **108**, 2–14 (2005).
5. N. Yamazoe, "New approaches for improving semiconductor gas sensors," *Sens. Actuators B Chem.* **5**, 7–19 (1991).
6. A. Ponzoni, E. Comini, I. Concina, M. Ferroni, M. Falasconi, E. Gobbi, V. Sberveglieri, and G. Sberveglieri, "Nanostructured metal oxide gas sensors, a survey of applications carried out at SENSOR Lab, Brescia (Italy) in the security and food quality fields," *Sensors* **12**(12), 17023–17045 (2012).
7. E. Comini, G. Faglia, M. Ferroni, A. Ponzoni, A. Vomiero, and G. Sberveglieri, "Metal oxide nanowires: Preparation and application in gas sensing," *J. Mol. Catal. Chem.* **305**(1–2), 170–177 (2009).
8. R. S. Devan, R. A. Patil, J.-H. Lin, and Y.-R. Ma, "One-dimensional metal-oxide nanostructures: recent developments in synthesis, characterization, and applications," *Adv. Funct. Mater.* **22**(16), 3326–3370 (2012).
9. H. Zheng, J. Z. Ou, M. S. Strano, R. B. Kaner, A. Mitchell, and K. Kalantar-zadeh, "Nanostructured tungsten oxide – properties, synthesis, and applications," *Adv. Funct. Mater.* **21**(12), 2175–2196 (2011).
10. P. R. Solanki, A. Kaushik, V. V. Agrawal, and B. D. Malhotra, "Nanostructured metal oxide-based biosensors," *NPG Asia Mater.* **3**(1), 17–24 (2011).
11. M. E. Franke, T. J. Koplin, and U. Simon, "Metal and metal oxide nanoparticles in chemiresistors: does the nanoscale matter?" *Small* **2**(1), 36–50 (2006).
12. I. D. Kim, A. Rothschild, B. H. Lee, D. Y. Kim, S. M. Jo, and H. L. Tuller, "Ultrasensitive chemiresistors based on electrospun TiO₂ nanofibers," *Nano Lett.* **6**(9), 2009–2013 (2006).

13. B. Schwenzer, L. Wang, J. S. Swensen, A. B. Padmaperuma, G. Silverman, R. Korotkov, and D. J. Gaspar, "Tuning the optical properties of mesoporous TiO₂ films by nanoscale engineering," *Langmuir* **28**(26), 10072–10081 (2012).
14. A. Rothschild and Y. Komem, "The effect of grain size on the sensitivity of nanocrystalline metal-oxide gas sensors," *J. Appl. Phys.* **95**(11), 6374–6380 (2004).
15. S. A. Sergeenko, P. S. Yaremov, V. N. Solomakha, and A. V. Shvets, "Effect of synthesis conditions on the structure and sorption properties of films based on mesoporous tin dioxide," *Theor. Exp. Chem.* **46**(3), 197–202 (2010).
16. X. Tang, K. Rimmel, X. Lan, J. Deng, H. Xiao, and J. Dong, "Perovskite-type oxide thin film integrated fiber optic sensor for high-temperature hydrogen measurement," *Anal. Chem.* **81**(18), 7844–7848 (2009).
17. M. Yang, J. Dai, X. Li, and J. Wang, "Side-polished fiber Bragg grating refractive index sensor with TbFeCo magnetooptic thin film," *J. Appl. Phys.* **108**(3), 033102 (2010).
18. J. Dai, M. Yang, Y. Chen, K. Cao, H. Liao, and P. Zhang, "Side-polished fiber Bragg grating hydrogen sensor with WO₃-Pd composite film as sensing materials," *Opt. Express* **19**(7), 6141–6148 (2011).
19. Z.-M. Qi, Z. Hao-shen, and I. Honma, "Mesostructured and mesoporous metal oxide films for optical waveguide-based gas sensor application," *Sensors 2004, Proceedings of IEEE* (2004), vol. 1313, pp. 1316–1319.
20. A. O. Dikovska, G. B. Atanasova, N. N. Nedyalkov, P. K. Stefanov, P. A. Atanasov, E. I. Karakoleva, and A. T. Andreev, "Optical sensing of ammonia using ZnO nanostructure grown on a side-polished optical-fiber," *Sens. Actuators B Chem.* **146**, 331–336 (2010).
21. Q. Yan, S. Tao, and H. Toghiani, "Optical fiber evanescent wave absorption spectrometry of nanocrystalline tin oxide thin films for selective hydrogen sensing in high temperature gas samples," *Talanta* **77**(3), 953–961 (2009).
22. S. Sumida, S. Okazaki, S. Asakura, H. Nakagawa, H. Murayama, and T. Hasegawa, "Distributed hydrogen determination with fiber-optic sensor," *Sens. Actuators B Chem.* **108**, 508–514 (2005).
23. X. Tang, J. Provenzano, Z. Xu, J. Dong, H. Duan, and H. Xiao, "Acidic ZSM-5 zeolite-coated long period fiber grating for optical sensing of ammonia," *J. Mater. Chem.* **21**(1), 181–186 (2011).
24. J. Zhang, M. Luo, H. Xiao, and J. Dong, "Interferometric study on the adsorption-dependent refractive index of silicalite thin films grown on optical fibers," *Chem. Mater.* **18**(1), 4–6 (2006).
25. X. Wei, T. Wei, J. Li, X. Lan, H. Xiao, and Y. S. Lin, "Strontium cobaltite coated optical sensors for high temperature carbon dioxide detection," *Sens. Actuators B Chem.* **144**, 260–266 (2010).
26. J. Zhang, X. Tang, J. Dong, T. Wei, and H. Xiao, "Zeolite thin film-coated long period fiber grating sensor for measuring trace chemical," *Opt. Express* **16**(11), 8317–8323 (2008).
27. Z. Gu, Y. Xu, and K. Gao, "Optical fiber long-period grating with solgel coating for gas sensor," *Opt. Lett.* **31**(16), 2405–2407 (2006).
28. T. Chuen-Lin, C. Tzu-Chung, C. Chun-Chia, C. Yu-Zong, and L. Wen-Fung, "Tuning sensitivity of liquid refractive index sensor based on side-polishing fiber Bragg gratings," in *Optical Fiber Communication and Optoelectronic Exposition and Conference, 2008. AOE 2008. Asia* (2008), pp. 1–3.
29. X. Chen, K. Zhou, L. Zhang, and I. Bennion, "Simultaneous measurement of temperature and external refractive index by use of a hybrid grating in D fiber with enhanced sensitivity by HF etching," *Appl. Opt.* **44**(2), 178–182 (2005).
30. Y. H. Kim, M. J. Kim, B. S. Rho, M.-S. Park, J.-H. Jang, and B. H. Lee, "Ultra sensitive fiber-optic hydrogen sensor based on high order cladding mode," *IEEE Sens. J.* **11**(6), 1423–1426 (2011).
31. A. Hartung, S. Brueckner, and H. Bartelt, "Limits of light guidance in optical nanofibers," *Opt. Express* **18**(4), 3754–3761 (2010).
32. G. Stewart, F. A. Muhammad, and B. Culshaw, "Sensitivity improvement for evanescent-wave gas sensors," *Sens. Actuators B Chem.* **11**, 521–524 (1993).
33. H. Peelaers, E. Kioupakis, and C. G. Van de Walle, "Fundamental limits on optical transparency of transparent conducting oxides: Free-carrier absorption in SnO₂," *Appl. Phys. Lett.* **100**(1), 011914 (2012).
34. D. S. Ginley and C. Bright, "Transparent conducting oxides," *MRS Bull.* **25**(08), 15–18 (2000).
35. K. J. Albert, N. S. Lewis, C. L. Schauer, G. A. Sotzing, S. E. Stitzel, T. P. Vaid, and D. R. Walt, "Cross-reactive chemical sensor arrays," *Chem. Rev.* **100**(7), 2595–2626 (2000).
36. P. Yang, D. Zhao, D. I. Margolese, B. F. Chmelka, and G. D. Stucky, "Block copolymer templating syntheses of mesoporous metal oxides with large ordering lengths and semicrystalline framework," *Chem. Mater.* **11**(10), 2813–2826 (1999).
37. S. Shao, M. Dimitrov, N. Guan, and R. Köhn, "Crystalline nanoporous metal oxide thin films by post-synthetic hydrothermal transformation: SnO₂ and TiO₂," *Nanoscale* **2**(10), 2054–2057 (2010).
38. V. N. Urade and H. W. Hillhouse, "Synthesis of thermally stable highly ordered nanoporous tin oxide thin films with a 3D face-centered orthorhombic nanostructure," *J. Phys. Chem. B* **109**(21), 10538–10541 (2005).
39. R. Landauer, "Electrical conductivity in inhomogeneous media," *AIP Conf. Proc.* **40**, 2–45 (1978).
40. L. Rosenfeld, *Theory of Electrons*, Vol. 1 in Selected Topics in Modern Physics (North-Holland, 1951), pp. xv, 119 p.
41. J. Isidorsson, C. G. Granqvist, K. von Rottkay, and M. Rubin, "Ellipsometry on sputter-deposited tin oxide films: optical constants versus stoichiometry, hydrogen content, and amount of electrochemically intercalated lithium," *Appl. Opt.* **37**(31), 7334–7341 (1998).

42. M. L. Åslund, J. Canning, M. Stevenson, and K. Cook, "Thermal stabilization of Type I fiber Bragg gratings for operation up to 600 ° C," *Opt. Lett.* **35**(4), 586–588 (2010).
 43. S. Bandyopadhyay, J. Canning, P. Biswas, M. Stevenson, and K. Dasgupta, "A study of regenerated gratings produced in germanosilicate fibers by high temperature annealing," *Opt. Express* **19**(2), 1198–1206 (2011).
 44. W. Johnstone, G. Thursby, D. Moodie, and K. McCallion, "Fiber-optic refractometer that utilizes multimode waveguide overlay devices," *Opt. Lett.* **17**(21), 1538–1540 (1992).
 45. W. Liang, Y. Huang, Y. Xu, R. K. Lee, and A. Yariv, "Highly sensitive fiber Bragg grating refractive index sensors," *Appl. Phys. Lett.* **86**(15), 151122 (2005).
 46. A. Lassesson, M. Schulze, J. van Lith, and S. A. Brown, "Tin oxide nanocluster hydrogen and ammonia sensors," *Nanotechnology* **19**(1), 015502 (2008).
-

1. Introduction

Metal oxides, amongst their many applications, are an important class of functional materials for chemical and bio sensing. Since the discovery of the sensing properties of these materials, a large variety of metal oxides and their doped variants have been extensively explored for highly sensitive conductometric sensors [1–5]. The basic origin and form of the resistivity response of chemiresistors can be linked to a change in free carrier concentration or free carrier mobility due to the charge transfer interactions that take place between the surface of the sensor and the chemisorbed species [4]. The optimization of the sensors selectivity, sensitivity, and response time to a specific analytes can still pose challenges to many of which doping with impurities does not yield adequate solutions. Nanostructuring metal oxides on the scale of tens of nanometers allow for the tailoring of their fundamental physical, electronic, and optical properties quite extensively for improved sensory performance [5–13]. The increase of the surface area of metal oxide nanostructures enhances the interactions between the oxide and the target species. The typical width of the gas modulated space charge region is between 1 and 10nm; therefore, nanostructuring on the scale comparable with this width provides high ratios between the modulated and non-modulated regions, allowing more effective utilization of the sensing material in comparison with thin film devices where the interacting volume is just the modulated width of its geometric surface [5, 12, 14, 15]. Lastly, the controlled nanostructuring on the tens of nanometer scale allows the tuning of the dielectric constants of metal oxides at will while maintaining sufficient scale separation between the dimensions of the nano features and the typical operating wavelengths (visible and near infrared, NIR) [13].

In addition to their extensive use in conductometric sensors, functional metal oxide nano-materials are excellent candidates for optical sensor platforms such as optical fiber. As a robust and scalable sensing technology well-suited for harsh environments, fiber optic sensors can provide unique opportunities and can perform in many conditions that are impossible for electronic sensors (e.g. high temperature, corrosive, strong electromagnetic fields, volatile organic/inorganic species). The integration of metal oxides with optical fiber constitutes a unique set of technical challenges. A critical way to improve the sensitivity of fiber optic sensors is to increase the interaction length between the metal-oxide coatings and the guided light. This in turn facilitates the accumulation of the response, whether refractive index or absorption based, leading to an increase in sensitivity. This is not a trivial issue given that the typical refractive indices of metal oxides ($n > 2.0$) are significantly higher than that of commercial silica fiber cores ($n \sim 1.46$). The optical interaction between the cores of silica fibers with higher index sensing films in close proximity can be detrimental to optical guiding.

2. Background and simulations

To date, successful demonstrations of fiber optic sensors utilizing metal oxides are realized by thin film coatings as in this domain the index compatibility issues can be mitigated [16–27]. Sensory materials such as metal oxides can be coated on D-shaped fiber, side polished fiber, or simply coated on the fiber cladding and can be combined with fiber Bragg gratings or long period gratings [17, 18, 20]. When combined with fiber Bragg gratings,

environmentally induced refractive index variations can be transduced into a wavelength shift of the grating peak [28, 29]. Some complex metal oxides have been shown to exhibit refractive index responses and can be combined with fiber Bragg gratings [16, 17]. When metallic coatings such as palladium or palladium and metal oxide composites are introduced with Bragg gratings, these act as strain transducers also exerting modifications on the grating peak [18, 30]. When long period gratings are introduced, these can act to increase the light interaction with functional coatings not in close proximity with the fiber core [16, 23]. A common factor amongst the demonstrated integrated fiber sensors is that when high refractive index functional materials are coated in close proximity with a lower index fiber core, they can only work in the thin film regime in order to minimize the intrinsic optical losses, which can be substantial. D-shaped fiber is a choice platform in optical fiber chemical sensing since the fiber core can be accessed while maintaining sufficient structure for mechanical stability. A schematic of D-shaped fiber coated with functional films in contact with the fiber core is illustrated in Fig. 1(a). As a rough estimate, the thickness of the high-index sensing films should be less than $\frac{1}{4}$ of the wavelength ($\lambda/4n$) to preserve guiding in the low-index fiber core [31]. This restriction on the film thickness (typically less than ~ 150 nm) places severe limitations on the interaction volume of the evanescent wave with the sensing medium. To explore the evanescent wave interactions, a detailed simulation is carried out. Figure 1(b) shows the detrimental effects when a high refractive index thick film (2- μm) is coated in contact with the fiber core, where most of the guided light is transferred to the fiber coating and is lost. Figure 1(c) illustrates the mode power distribution in the device when the refractive index of the film (1.461) is slightly lower than that of the fiber core (1.468), a configuration in which light guiding is preserved.

The dependence of the confinement factors on the film thickness and the refractive indices were explored by finite element analysis. Figure 1(d) shows the refractive index of the film and the percentage of the guided light propagating in the thin film as the function of the film thickness, when the metal oxide coating does not disturb the guided mode in the fiber core. This is defined as the fiber maintains a constant effective index ($n_{\text{eff-sensing}} \approx n_{\text{eff-uncoated}} = 1.464$). Figure 1(d) indicates that when the refractive index of the film is equal to that of the fiber cladding, the maximum evanescent interaction (1.6%) is achieved with minimal mode mismatching losses. The simulation in Fig. 1(d) also indicates that a metal oxide coating with a nominal index of 2 would require the coating thickness to be 100nm or less, in order to preserve guiding in the D-shaped fiber core, yielding a confinement factor of 0.2%. In many reports it is not clear whether the film thicknesses were optimized to return the fiber to its unmodified operating condition, ensuring that the intrinsic losses are minimal. Therefore, the improvements we state are in regard to optimized coatings and in practice much greater improvements are possible.

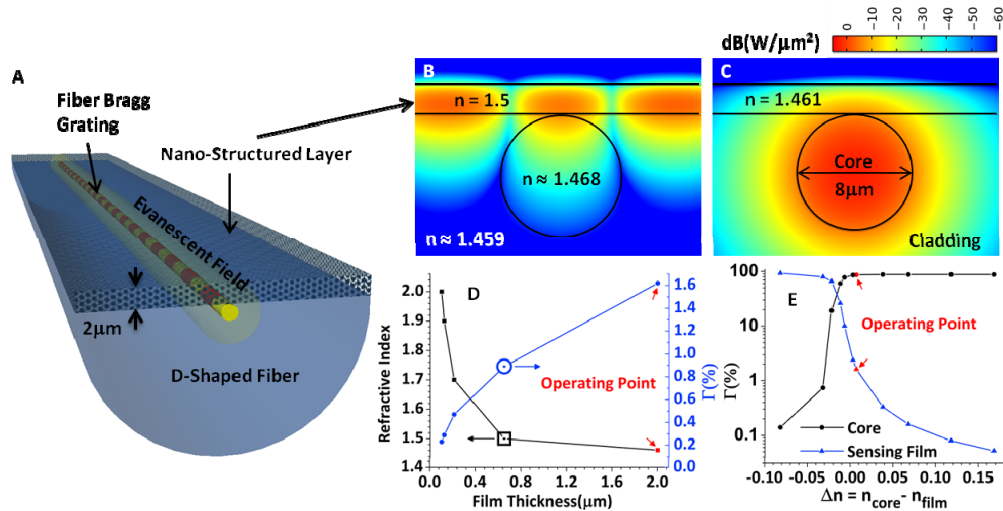


Fig. 1. A: Schematic of D-shaped fiber coated with nanostructured SnO₂, with an in-fiber Bragg Grating. B-C: Simulations of the power distributions of the fundamental mode for a coating refractive index of 1.5 (index above the value of the core) and 1.461 (Nanostructured SnO₂ used for the experiment). D: Simulations of various coating refractive indices and the associated confinement factors as functions of film thickness while maintaining the mode-match condition. The thicknesses are those that maintain the fiber's n_{eff} to its original value. E: The confinement factors as functions of the index difference between the core and the sensing film ($\Delta n = n_{core} - n_{film}$) at a coating thickness of 2 μm for small film index variations. The above simulation were examined for an operating wavelength of $\lambda = 1.55 \mu\text{m}$.

In this paper, we demonstrate that the complications and limitations of using metal oxides with high dielectric constants can be overcome by replacing thin film designs with refractive index tailored 3D nanomaterials [32]. We demonstrate for the first time that the refractive index of SnO₂ can be tailored “at will” to meet the refractive index compatibility requirements while at the same time maximizing the interacting optical power by eliminating any restrictions on thickness and minimizing the unwanted optical losses. The use of a structure directing agent in the wet chemical preparation of SnO₂ provides an engineering opportunity on the tens of nanometer scale where, by controlling the structure directing component, the refractive index can be adjusted in accordance with effective medium theory. Reducing the refractive index below the refractive index of the fiber core removes the thickness constraints, allowing the coating of thick 3D nanomaterials while maintaining mode matching between the sensing and non-sensing regions of the fiber for intrinsic loss optimized designs. This allows the coating of films with arbitrary thicknesses that greatly enhance the evanescent wave interactions.

The effects of small variations in the refractive indices, near the optimal refractive index, on the guided wave confinement factors for the core and sensing film were examined by simulation for a 2- μm thick coating, shown in Fig. 1(e). When the refractive index of the metal oxide is slightly smaller than that of the fiber core, enhancements that are greater than 8 times the confinement factor for evanescent wave interaction can be achieved in the sensing films as compared to optimized thin film coatings. Figure 1(e) shows that when the refractive index of the coating is slightly larger than that of the fiber core, a total guided light energy transfer to the fiber coating will occur, destroying the guiding condition. The simulations demonstrate the challenges and the importance of refractive index engineering of functional coatings, which is the subject of this paper.

In addition, the tailoring of the refractive indices allows the many previously explored benefits of metal oxide nanostructures to be incorporated into optical fiber sensors such as

increased surface to volume ratios and higher ratios between the modulated and non-modulated regions yielding faster and more sensitive sensors.

In the optical domain, it is not easy to predict the type of the expected response or combination of responses for metal oxide nanostructures with features comparable to the gas modulated space charge region's width, for which the surface effects dominate. It is well known that a conduction increase/loss is to be expected, depending on the type of the analyte (reducing/oxidizing) and the type of the metal oxide (n/p-type). This, in the optical domain at NIR, for SnO₂, will show up as absorption based on Drude's theory as in this regime the response is dominated mostly by free electron absorption [33, 34]. Based on the theory, however, it is not clear whether there should be an expected measurable change in the real part of the refractive index. In addition to absorption, a measurable modulation in the real part of the refractive index could potentially provide another method in cross sensitivity discrimination, which is a common problem of metal oxide sensors [35]. To probe the optical sensory mechanisms of the SnO₂ nanomaterial, this paper uses a fiber Bragg grating in D-shaped fiber to simultaneously measure the optical losses and the refractive index changes from room temperature up to 500°C in response to NH₃. In this work, SnO₂ was used as an example for refractive index tailoring through controlled nanostructuring. However, we point out that this approach is general and should be transferable to optimizing the response of optical fiber sensors integrated with many metal oxide based materials.

3. Results and discussions

In the wet chemical synthesis of the precursor, Pluronic F-127, a triblock copolymer was used as the structure directing agent for the nano-engineering of SnO₂ [15, 36–38]. By controlling its mole fraction, the porosity of the SnO₂ is controlled on the tens-of-nanometers scale to tailor the refractive index of the nano-material. In prior, this method was shown effective towards modifying the resistive and surface properties of metal oxides.

The sol gel solution used in the fabrication of the nanomaterial consisted of SnCl₄, Pluronic F-127, HCl, and Ethanol with a molar ratio of 1:0.04:7.71:39.58 (ACS Reagent Grade, Sigma Aldrich). After mixing, the solution was stirred for 3 hours, followed by a settling period of 24 hours. In the preparation of the precursors, many authors employ careful humidity control in processing these materials. We found that the hydrolysis can be substantially slowed upon exposure with ambient air by adjusting the pH value of the precursor to ~0.5 using HCl [37]. The slowing of the hydrolysis provided higher quality films when spin coated for refractive index measurements.

To characterize the refractive index, the precursor was spun onto a silicon wafer at 2500 RPMs, heat treated and measured using an Ellipsometer (Jobin Yvon Uvisel Spectroscopic Ellipsometer). The Lorentz single oscillator model along with Bruggeman's effective medium theory was used in the fitting process to estimate the refractive index of the nanomaterial [39, 40]. Parameters were measured in the range of 400-800nm after which the model was used to extend the refractive indices to 1600nm. Extrapolating the refractive index in this manner should provide reasonable values as it has been shown that the variation in the dielectric constant of SnO₂ at higher wavelengths is slowly varying [41].

Figure 2 shows the fitted from direct measurement (400-800nm) and extrapolated (800-1600 nm) refractive indices of various forms of SnO₂. The refractive index of bulk, fully dense SnO₂ is also presented as a reference (built into the software package of the Ellipsometer). A 100-nm thick SnO₂ thin film prepared by sputter coating (estimated porosity of around 3-5%) is also included for comparison. Refractive index measurements of three nanostructured SnO₂ films are presented in Fig. 2 with varying contents of Pluronic F-127 (SnO₂ – A, B, and C). We determined a volume fraction of about 60% for nanostructured SnO₂ –B (nanomaterial used in the construction of the sensor). At 1550nm, the wavelength of interest, it has a refractive index of 1.461, which is slightly smaller than the refractive index of the fiber core (1.468).

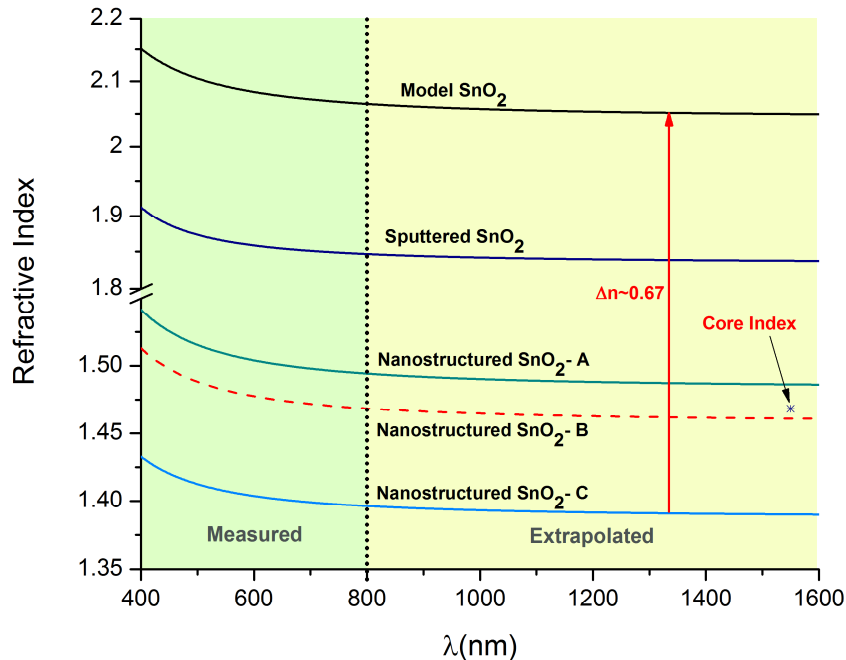


Fig. 2. The refractive indices of various forms of SnO₂. Sputtered SnO₂ was sputter coated at a thickness of 100nm. SnO₂-A is with mole fraction 1:0.008:2:21.74, B with mole fraction 1:0.04:7.71:39.58, and C with mole fraction 1:0.016:2:21.7. The mark labeled “Core Index” is an estimate of the refractive index of the core of the fiber (1.468) and SnO₂-B, used to fabricate the sensor, has an estimated refractive index of 1.461 at $\lambda = 1.55\mu\text{m}$.

A cross section SEM image of the sensor in Fig. 3(a) shows that the thickness of the film directly above the core is roughly $2\mu\text{m}$. Sufficiently thick for trapping most of the evanescent energy in the interaction region, as calculations show that greater than 98% of the radiant intensity of the evanescent wave is in the coating. Cross-sectional TEM samples were prepared through standard focused ion beam (FIB) lift-out procedures for SnO₂ deposited on the D-shaped fiber, inset of Fig. 3(b). A protective layer of Pt was deposited on the surface prior to sectioning. A tungsten-probe tip was used for sample lift-out and electron transparency was obtained over an approximately $10\mu\text{m}$ wide region for the entire film thickness. Scanning transmission electron (STEM) images of Fig. 3(b) clearly show a large degree of film porosity through z-contrast with features of about $\sim 20\text{-}50\text{nm}$ in diameter. Bright field TEM imaging shows an average SnO₂ grain size of approximately 10nm shown in Fig. 3(c) and a Fast Fourier Transform (FFT) obtained from the high resolution TEM image indicates an underlying cassiterite crystal structure shown in Fig. 3(d).

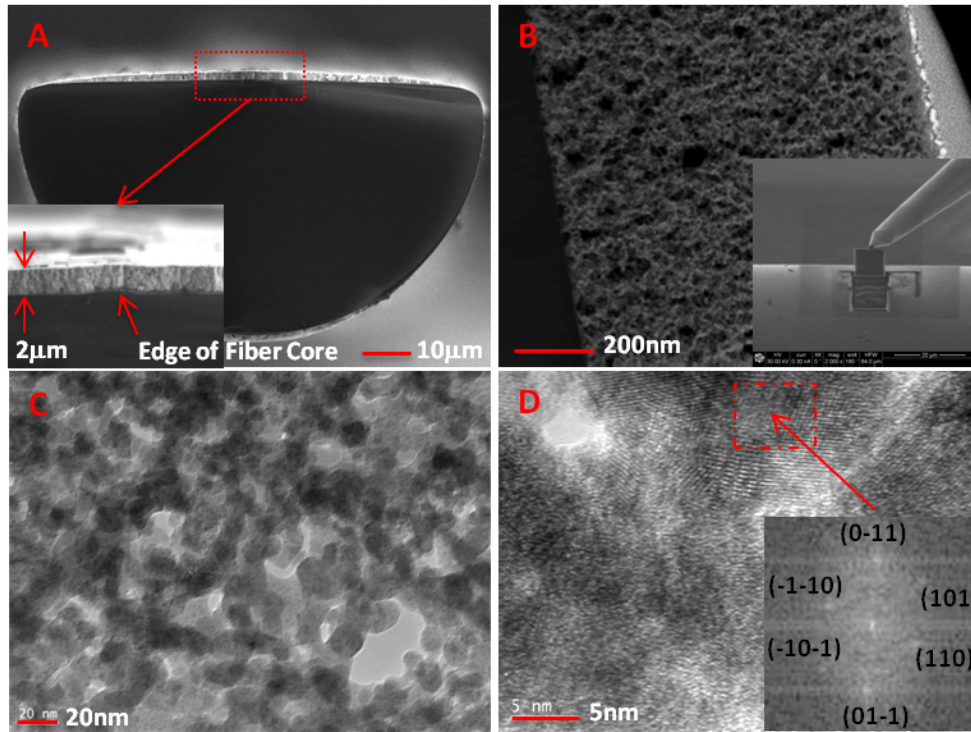


Fig. 3. A: Cross sectional SEM image of the constructed sensor. B: STEM image of the entire film thickness along with an SEM image (inset) illustrating the FIB lift-out. C: Bright field TEM image illustrating an average SnO_2 grain size of approximately 10nm. D: High resolution TEM imaging of the crystal structure of SnO_2 with FFT inset indexed to the [1-1-1] zone axis of the cassiterite crystal structure.

To produce the fiber Bragg grating, D-shaped fiber was first soaked in high pressure hydrogen at 1600 psi for 2 weeks. A type II Fiber Bragg Grating (FBG) was inscribed by a phase mask (2.5x1cm with 1060nm period) with a 248nm KrF laser source (GSI Lumonics PM-844) with a cumulative fluence of $\sim 6,000$ pulses at $\sim 50\text{mJcm}^{-2}$ [42, 43]. The FBG sensor was then annealed at 120°C for 24 hours to diffuse out all the residual hydrogen. Prior to coating the precursor, the D-fiber with the FBG was etched with a buffered HF solution for 21 minutes to remove 3 μm cladding material (5:1 40% NH_4F to 49% HF ACS Reagent Grade, Sigma Aldrich), exposing the core on the flat side of the fiber. The fiber was coated by pulling it through the precursor at an approximate rate of 5mm/s. The coated sample was then exposed to a temperature treatment which started by drying at 80°C for 3 hours. Next, the temperature was increased at 5°C/minute to 130°C and held for 1 hour. Followed by ramping (3°C/minute) to 600°C, where it was held for 2 hours. Afterwards, the sample was cooled to room temperature at a rate of 3°C/minute.

The schematic of the gas sensing experimental setup is shown in Fig. 4(a). The fiber sensor coated with the reduced index SnO_2 was exposed to a constant flow(200 SCCM) of 10% NH_3 and 90% N_2 mixture at atmospheric pressure for 3 minutes, followed by a 3 minute recovery period in dry air(200 SCCM). A change in the real part of the refractive index of the 7-cm long fiber coating is monitored by the reflection peak of the FBG sensor using a broadband light source (EBS-7210 Er^{3+} Broadband, MPB Technologies) and an Optical Spectrum Analyzer (Agilent 86140B). Another Optical Spectrum Analyzer (Ando 6317B) was used to monitor transmission spectra of the coated D-fiber to measure the real-time optical loss. The FBG reflection peak disappears immediately upon the coating of the

precursor due to its high refractive index in comparison with the core of the fiber. A short time after raising the temperature above 200°C, the grating peak begins to return due to the removal of the structure directing agent, indicating the reduction of the refractive index.

A change in the effective index Δn_{eff} of the guided mode can be measured directly by monitoring shifts in the FBG peak $\Delta\lambda$ as $\Delta n_{\text{eff}} \approx \Delta\lambda/2\Lambda$, where Λ is the grating period [17, 44, 45]. Any displacements in the peak under stable temperature conditions, which we could detect down to 10-pm levels, would be indicative of a refractive index change in the nanostructure. An example of the measurement of the wavelength of the resonant peak is given in Fig. 4(b), at room temperature. In measuring the reflected power from 25 to 500°C, we do not observe any shifts in the resonance peak due to the adsorption of NH_3 . Given the sensitivity of our instruments and the 1.62% optical confinement factor in the sensing film, we estimate that any modulations in the refractive index is smaller than $\sim 5 \times 10^{-4}$.

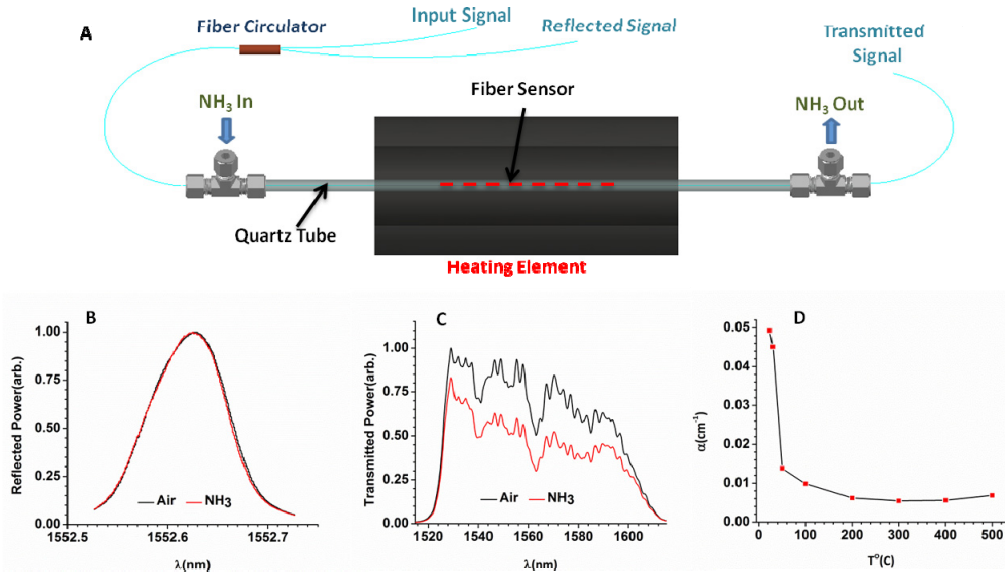


Fig. 4. A: Experimental schematic. B: FBG resonant peak response of the sensor at room temperature to 10% NH_3 . No shift in the resonance peak is observed, indicating that there is not a significant refractive index response. C: Transmission analysis of the response of the sensor at room temperature to 10% NH_3 , indicating a strong loss in the transmitted power. D: The total absorption coefficient of the integrated component as a function of temperature.

The above exposure conditions produce a significant optical loss evident in the transmission measurement, for which we measured about a 30% reduction in the transmitted optical power around 1.5 μm , shown in Fig. 4(c). The optical loss coefficient of the device in this configuration is $\alpha_{\text{Sensor}} = 0.049 \text{ cm}^{-1}$. Given that 1.6% of guided light interacts with the metal oxide coating, the overall absorption coefficient for SnO_2 materials in reaction with NH_3 is $\alpha_{\text{SnO}_2} = 3 \text{ cm}^{-1}$. The loss appears to be uniform across the transmission measurement spectra. A maximum in the transmitted power was observed at room temperature after which it shortly declined with the increase of the temperature as shown in Fig. 4(d). This result is contradictory to the general thermal dependence of chemiresistors as their temperature response has a maximum sensitivity at higher temperatures, typically between 200 and 500°C; therefore, many devices tend to hold their SnO_2 sensor in that temperature range for peak sensitivity. On the other than, SnO_2 nanowires have been reported to have thermal characteristics different from their bulk counterpart as do SnO_2 nanoclusters [6, 7, 46]. From this, we speculate that the anomalous temperature response might be due to the current nanostructure.

4. Conclusions

In summary, we presented, for the first time, to the best of our knowledge, a refractive index engineered SnO₂ functional film integrated with optical fibers to maximize the evanescent interactions for sensing applications. The refractive index was successfully adjusted by a triblock copolymer, Pluronic F-127 which acted as a structure directing agent in the manufacture of the SnO₂ nanomaterial. Through the integration of nano-engineered metal oxide with high-temperature stable fiber Bragg grating, this work examined both refractive index and absorption modulation of the metal oxide based sensors at both the room temperature and at high temperature up to 500°C for energy applications.

Results presented in this paper reveal that conductivity changes in metal oxide nanomaterials previously reported in electronic sensors lead to significant increases in optical absorption as predicted by Drude's theory. On the other hand, although D-shaped fiber sensors are known for their sensitivities to the environmental refractive index changes, measurements reported in this paper shows very small refractive index changes occurred in metal oxide nanomaterials in reaction with NH₃, which is below the sensitivity of our instruments ($\Delta n < 5 \times 10^{-4}$).

We believe that this work can provide important guidance for the design of optical fiber sensors employing metal oxides as sensory transducers. The metal oxide nanomaterial synthesis scheme presented in this paper allows the adaptation of the many advances achieved in metal oxide conductometric sensors, such as specific dopings, high surface to volume ratios, and specific annealing conditions known to affect grain and crystallite sizes. These properties are all known to provide great enhancements in sensitivity, selectivity, and response times. Fiber sensors designed to measure small optical absorption such as cavity ring-down spectroscopy is better suited to harness the strong optical absorption for highly sensitive chemical sensing when integrated with reduced index metal oxide nanomaterials.

Acknowledgments

This work was supported by the National Science Foundation (CMMI-1054652 and CMMI-1109977) and the Department of Energy (DE-FE0003859). This report was prepared as an account of work sponsored by an agency of the United States Government. Neither the United States Government nor any agency thereof, nor any of their employees, makes any warranty, express or implied, or assumes any legal liability or responsibility for the accuracy, completeness, or usefulness of any information, apparatus, product, or process disclosed, or represents that its use would not infringe privately owned rights. Reference herein to any specific commercial product, process, or service by trade name, trademark, manufacturer, or otherwise does not necessarily constitute or imply its endorsement, recommendation, or favoring by the United States Government or any agency thereof. The views and opinions of authors expressed herein do not necessarily state or reflect those of the United States Government or any agency thereof.